

# GridFF: Efficient Simulation of Organic Molecules on Rigid Substrates

Indranil Mal,<sup>\*,†</sup> Milan Kočí,<sup>†,‡</sup> Paolo Nicolini,<sup>†</sup> and Prokop Hapala<sup>\*,†</sup>

<sup>†</sup>*FZU - Institute of Physics of the Czech Academy of Sciences  
Na Slovance 2, Prague, 18 200, Czech Republic*

<sup>‡</sup>*Faculty of Nuclear Sciences and Physical Engineering, Czech Technical University in  
Prague, Břehová 7, Prague, 115 19, Czech Republic*

E-mail: mal@fzu.cz; hapala@fzu.cz

## Abstract

We present GridFF, an efficient method for simulating molecules on rigid substrates, derived from techniques used in protein-ligand docking in biochemistry. By projecting molecule-substrate interactions onto precomputed spatial grids with tricubic B-spline interpolation, GridFF reduces the computational cost by orders of magnitude compared to traditional pairwise atomistic models, without compromising the accuracy of forces or trajectories. The CPU implementation of GridFF in the open-source FireCore package provides a 100-1000 $\times$  speedup over all-atom simulations using LAMMPS, while the GPU implementation – running thousands of system replicas in parallel – samples millions of configurations per second, enabling an exhaustive exploration of the configuration space of small flexible molecules on surfaces within minutes. Furthermore, as demonstrated in our previous application of a similar technique to high-resolution scanning probe microscopy, GridFF can be extended beyond empirical pairwise potentials to those derived from *ab initio* electron densities. Altogether, this unlocks accurate high-throughput modeling of molecular self-assembly, adsorption, and scanning probe manipulation in surface science.

## 1 Introduction

The structural characterization and design of organic/inorganic interfaces represent a critical challenge across multiple research and technological fields, including friction and lubrication,<sup>1–3</sup> molecular electronics,<sup>4</sup> photovoltaics,<sup>5</sup> and scanning probe microscopy (SPM).<sup>6</sup> The interaction of organic molecules with surfaces of inorganic crystals plays a key role in the development of molecular nanotechnology comprising self-assembled monolayers,<sup>7</sup> 2D molecular crystals,<sup>8</sup> covalent organic frameworks,<sup>9</sup> and also for the emerging field of on-surface chemistry.<sup>10</sup> Complex molecular nanostructures are one of the most promising building blocks for next-generation computational devices such as molecular electronics,<sup>11</sup> photonics,<sup>12</sup> and quantum cellular automata.<sup>13</sup>

The formation of such structures is primarily governed by non-covalent interactions between organic molecules and the templating effects of the inorganic substrate. However, predicting the absorption configurations of molecules on surface and self-assembled layers remains an open challenge, akin crystal structure prediction in pharmaceuticals<sup>14</sup> and protein folding in biochemistry.<sup>15</sup> The challenge of designing such structures, especially from flexible molecules, arises from the curse of dimensionality, related to soft internal degrees of freedom (*e.g.*, torsions along single bonds), which drastically ex-

pands their configuration space. Fortunately, the interaction with rigid inorganic substrates can constrain this structural freedom, enabling more systematic and rational design of self-assembled motifs from first principles.

Crystalline inorganic substrates also provide an ideal, well-defined support for the experimental construction and study of complex nanosystems.<sup>16</sup> Unlike bulk solids or liquid solutions, surfaces allow unobstructed access to functional molecular components and atomic-level control through SPM techniques. SPM is not only an indispensable tool for imaging nanostructures with atomic resolution,<sup>17</sup> but it also offers the potential to construct complex supramolecular structures by direct manipulation.<sup>18</sup> However, the optimal control of molecular degrees of freedom through interactions with an atomic force microscope (AFM) or a scanning tunneling microscope (STM) tip remains a major challenge, heavily dependent on atomistic simulations. Without such simulations, SPM manipulation becomes a blind trial-and-error process, as the instrument provides minimal experimental information about molecular configurations during manipulation.<sup>19</sup> Recent efforts to automate this laborious process involve reinforcement learning for robotic AFM/STM machines.<sup>20–22</sup> However, training such robotic systems through direct experimentation is prohibitively expensive and time-consuming due to the vast number of required training examples. This underscores the need for a specialized virtual training nanophysics engine – akin to NVIDIA’s Isaac physics engine<sup>23</sup> – capable of generating the data needed for training robotic manipulation of nanoscale objects, possibly parallelized on graphics processing units (GPU).

An even more ambitious challenge is the computational molecular design of organic molecules that deterministically self-assemble into target patterns or shapes on a substrate, *e.g.* driven by hydrogen bond formation.<sup>24</sup> In this case, whilst chemical intuition may suffice for designing simple structures based on one or two hydrogen bonds from rigid molecules, creating complex patterns requires molecules with significantly greater structural informa-

tion and an inverse computational design. Notable examples include biopolymers such as DNA, RNA, and proteins, whose self-assembly can be computationally designed using automated tools, often leveraging machine learning approaches like AlphaFold.<sup>25</sup> However, training such design tools requires extensive databases of self-assembled (folded) structures, which in biochemistry are obtained from experimental data or atomistic simulations.<sup>26</sup> In the domain of molecular surface science, no comparable database currently exists, and constructing such a database for newly designed molecules using experimental methods would be prohibitively expensive. Therefore, softwares capable of efficiently predicting self-assembled patterns for a broad range of novel molecules are essential for the rational design of molecular nanostructures on surfaces.

Moreover, the structure of molecular assemblies at finite temperatures is influenced not only by enthalpy, but also by entropic contributions. For soft, flexible molecules, entropy can play a particularly significant role. The temperature dependence of the entropy term in the Gibbs free energy ( $\Delta G = \Delta H - T\Delta S$ ) is crucial for estimating the melting temperature of self-assembled structures and determining annealing conditions for their reversible formation. These are key parameters in computational design, particularly for larger self-assembling molecular templates akin to DNA fragments or oligopeptides. However, the computational estimation of entropy and free energy requires an exhaustive configuration sampling of the partition function, which is extremely demanding – especially when one aims at screening a large number of candidate molecules.

Consequently, both SPM manipulation of molecules on solid substrates and their self-assembly ultimately face the same fundamental challenge: exploring a vast configuration space of soft organic molecules while simultaneously describing their interactions with the substrate (and potentially with an AFM/STM tip) efficiently. The sheer size of this configuration space renders *ab initio* methods computationally unfeasible, necessitating the use of classical force fields. Unfortunately, many exist-

ing methods for molecular configuration exploration, such as CREST<sup>27</sup> – designed for systems in gas or liquid phases – cannot be directly applied to molecules on surfaces. Likewise, state-of-the-art force fields, like AMBER,<sup>28</sup> CHARMM,<sup>29</sup> GROMOS<sup>30</sup> and OPLS<sup>31</sup> (which can be used on general-purpose simulation programs such as AMBER,<sup>32</sup> CHARMM,<sup>33</sup> GROMACS,<sup>34</sup> LAMMPS<sup>35</sup> and NAMD<sup>36</sup>), are primarily optimized for biological molecules in aqueous environments, making efficient simulations of molecular interactions with substrates highly challenging.

To address these limitations and provide an efficient tool for SPM manipulation and self-assembly of small organic molecules on ionic substrates, we have developed a new classical force field simulation software.<sup>37</sup> The software we introduce here is optimized for efficient parallel configuration sampling, accelerated using modern GPUs, and incorporates a specialized grid-projected force field (GridFF) to enhance the description of molecule-substrate interactions. This approach, which is the main focus of this publication, enables precise and computationally feasible predictions of molecular self-assembly and manipulation on inorganic surfaces, bridging the gap between theoretical modeling and experimental nanostructure design.

## 2 Motivations

Simulating organic molecules on inorganic substrates, even using classical force fields, can be relatively costly, particularly when using large supercells comprising a large number of atoms. In such systems the number of substrate atoms  $n_S$ , replicated across multiple unit cells, far exceeds the number of atoms of the organic molecules  $n_M$  being studied, leading to substantial computational overhead. There is more than one reason why one has to use large supercells. First of all, in order to properly model a crystal slab, several atomic layers shall be considered. In complex surface reconstructions, the unit cell itself may be also very large. Moreover, if one aims to simulate an isolated molecule on a surface, the sizes of the cell must be large

enough to avoid artifacts due to the interaction between the molecule and its periodic images. On the other hand, even in the case of periodic systems such as self-assembled monolayers, one has to deal with the intrinsic incommensurability between the two lattices. For all these reasons, the typical case is  $n_S \gg n_M$ . Furthermore, many classical force fields parameterizations struggle to simultaneously capture the nuances of both molecule-substrate interactions, and bulk mechanics of the crystal. For this reason, in such simulations, it is a common practice to fix the position of the substrate atoms, or at least the bottom atomic layers. Even in this case, the computational overhead is not reduced in most implementations as the number of pairwise interaction scales quadratically with the total number of atoms in the supercell  $(n_M + n_S)^2$ . Even if pairwise interactions between the atoms of the substrate can be eliminated (which is generally a non-standard feature in classical force field programs<sup>38</sup>), the computational cost of evaluating  $n_M n_S$  pairwise interactions between the molecule and the substrate dominates over the  $n_M^2$  calculations required to describe the interactions between atoms in the molecule.

Electrostatics interactions, due to their slow convergence in real-space calculations, require a different treatment. They are usually addressed by evaluating the interactions in the Fourier space using techniques derived from the Ewald summation,<sup>39</sup> such as the Particle-Mesh Ewald (PME) method.<sup>40</sup> However, achieving a satisfactory accuracy requires a large plane-wave cutoff and a correspondingly dense grid, making PME a frequent bottleneck in periodic classical force field calculations. This computational cost increases with the supercell size as  $O(N \log(N))$  (where  $N$  is the number of grid points).

GridFF, inspired by a similar method used typically for rigid protein-ligand docking,<sup>41,42</sup> offers an alternative approach designed to address these limitations. Unlike traditional force fields, which evaluate all pairwise interactions and PME on-the-fly, GridFF precalculates the molecule-substrate interaction potential on a grid before the actual simulation is performed.

This precalculated grid, representing the interaction potential, is then simply interpolated during the simulation. This largely decreases the computational cost, and allows one to use denser grids, larger supercells, and more complex force fields without added computational cost. In addition to this, GridFF does not necessarily need to be constructed from pairwise potentials (*e.g.*, as in the D3 van der Waals corrections,<sup>43</sup> where three-body terms are considered), but can also be computed directly from electron densities obtained from *ab initio* wavefunctions, as it is routinely done in the so-called full density based model (FDBM) in atomic force microscopy simulations.<sup>44,45</sup>

Whilst the computational cost of a traditional pairwise potential scales quadratically with the number of particles in the system, and Ewald summation scales logarithmically (albeit with a significant prefactor), the cost of evaluating the GridFF potential through interpolation remains essentially constant. Although cache memory effects might subtly influence the performance for large grids, the computational complexity of the interpolation algorithm itself is independent of the grid size, offering significant potential for speedup when the molecule-substrate interaction is the computational bottleneck.

### 3 Principles

Grid-based potentials for the description of non-covalent interactions, such as Coulomb and Lennard-Jones, are routinely used in computational biochemistry codes for protein-ligand docking.<sup>46–48</sup> Nevertheless, here we briefly recall the approach originally published by Goodford.<sup>49</sup> The core idea lies in the assumption that the total interaction energy  $E$  between the molecule and the substrate can be decomposed into a sum of atomic contributions

$$E = \sum_i E_i(r_i, t_i, Q_i), \quad (1)$$

where  $r_i$ ,  $t_i$  and  $Q_i$  are the position, type and charge of the molecular atom  $i$ . Each term  $E_i$  can be interpolated from the grid potential us-

ing efficient techniques such as 3D trilinear<sup>50</sup> or tricubic splines,<sup>51</sup> which are particularly well-suited for implementation on GPU hardware. In ligand docking applications, the trilinear approximation prevails due to the minimal computational cost, despite the fact that it cannot provide high quality forces.<sup>52</sup> Grid potentials are then typically used to evaluate energy-based scoring function only, not to run molecular dynamics simulations or force-based optimizations.<sup>53</sup> Moreover, these potentials are often artificially softened to effectively mimic flexibility and thermal fluctuations of the protein at room temperature.<sup>54</sup> In some approaches, the grid force fields are used for mapping free energy profiles using Monte Carlo sampling at finite temperature.<sup>55–57</sup> In such situations, eventual inaccuracies in energy and force evaluation are smeared out by thermal fluctuations. This is in contrast to our applications of GridFF for force-based dynamical simulations at low temperature, where molecule precisely follows the potential energy surface (PES), and a delicate balance between the gradient of the PES and the driving force (from the AFM tip) determines bifurcations of the trajectory near saddle points. Therefore, in this work we opted for higher order interpolation (*i.e.*, tricubic B-splines), and much finer grids ( $\sim 0.1$  Å) to obtain high-quality forces. We found that even this computationally more intensive settings for GridFF provide significant speedups compared to all-atom potentials.

As already mentioned, a grid-based potential can be constructed using any desired method, namely a direct projection of pairwise potentials, a fitting procedure based on density functional theory (DFT) calculations, or a machine-learned potential. In its simplest form, GridFF approximates the molecule-substrate interaction by projecting typical non-covalent pairwise potentials – such as Coulomb, Morse, or Lennard-Jones – onto the grid. In the general case, this involves evaluating the potential

$$E_i(r_i, t_i, Q_i) = \sum_j V_{ij}(|r_i - r_j|, t_i, t_j, Q_i, Q_j)$$

for each atomic type  $t_i$  of the molecular atoms



interacting with all substrate atoms  $j$ . In principle this is doable; nevertheless, it can be very memory demanding, as one may end up with tens or hundreds of grids  $V_{ij}$  for all possible  $ij$  combinations, each accounting hundreds of megabytes of memory.

Another consideration to take into account is the efficiency of cache memory (which decreases when reading from distant memory addresses), finally making this formulation practically useless. For this reason, grid-based potentials often<sup>41,42,54</sup> (but not always<sup>50,51,58</sup>) rely on various factorization schemes where the parameters of the ligand atoms (the molecular adsorbate in our case) can be factored out of the summation over the substrate atoms. This can be done easily for Coulomb and Morse potential with Lorentz-Berthelot mixing rules. For electrostatics interactions, this is trivial:

$$\begin{aligned} E_i^C(r_i, Q_i) &= \sum_j \frac{Q_i Q_j}{|r_i - r_j|} = Q_i \sum_j \frac{Q_j}{|r_i - r_j|} \\ &= Q_i V_i^C(r_i). \end{aligned} \quad (2)$$

The factorization for a Morse potential can be done by applying basic properties of the exponential function (*i.e.*,  $e^{a+b} = e^a \cdot e^b$ ) separately to the repulsive (Pauli) and attractive (London dispersion) parts:

$$\begin{aligned} E_i^M(r_i, t_i) &= \sum_j \varepsilon_i \varepsilon_j e^{-2\alpha(|r_i - r_j| - R_i - R_j)} \\ &\quad - 2 \sum_j \varepsilon_i \varepsilon_j e^{-\alpha(|r_i - r_j| - R_i - R_j)} \quad (3) \\ &= P_i(t_i) V_i^P(r_i) + L_i(t_i) V_i^L(r_i), \end{aligned}$$

where

$$\begin{aligned} P_i(t_i) &= \varepsilon_i e^{2\alpha R_i} \\ L_i(t_i) &= -2\varepsilon_i e^{\alpha R_i} \\ V_i^P(r_i) &= \sum_j \varepsilon_j e^{-2\alpha(|r_i - r_j| - R_j)} \\ V_i^L(r_i) &= \sum_j \varepsilon_j e^{-\alpha(|r_i - r_j| - R_j)}. \end{aligned} \quad (4)$$

Therefore, the three grids defined above ( $V_i^C$ ,  $V_i^P$  and  $V_i^L$ ) do not carry any dependence on molecular atomic types nor charges. This

means that once the grids have been calculated, then it is possible to simulate the interaction with any molecule, without the need of any other precomputation. It is also worth noting that the GridFF approach does not pose any restriction on the number of substrate atom types. Finally, during the evaluation of energies and forces, we simply perform the interpolation of the three separately stored grids (with the coefficients in Eq. 4) using Eqs. 1, 2 and 3, and considering that  $E = \sum_i E_i^C + E_i^M$ .

## 4 Periodicity and long-range electrostatics

As anticipated in the previous section, the treatment of long-range Coulomb interactions in classical force field simulations requires some attention. A naive evaluation of electrostatic energy via direct pairwise summation does not converge for periodic systems, and even in neutral systems, electrostatic forces converge only very slowly with distance, consuming a relevant amount of computational resources. Fortunately, periodic boundary conditions (PBC) allow the use of efficient reciprocal-space summation techniques based on the Ewald summation. For example in PME,<sup>40</sup> atomic charges are projected onto a grid as a charge density  $\rho(\vec{r})$ , and the electrostatic potential is calculated in the reciprocal space via  $V(\vec{k}) = \rho(\vec{k})/|\vec{k}|^2$ , using fast Fourier transforms (FFT) to switch between real and reciprocal space representations.

The PME algorithm is so efficient that it is often used even for systems that are not naturally periodic (*e.g.*, proteins in water, or a single molecule on a surface), at the cost of introducing artificial interactions between periodic images of the system. Using PME for surfaces is further complicated by the lack of periodicity in the  $z$ -direction. A well-established and computationally efficient solution (used both in LAMMPS and FireCore) is to add a sufficient vacuum padding above the surface and apply monopole and dipole corrections to the resulting 3D-periodic solution, assuming that higher-order multipole contributions decay rapidly.<sup>59</sup> For pristine surfaces, due to the exponential de-

cay with  $z$  of the electrostatic potential of the substrate and the absence of molecular multipoles, this approach can be particularly efficient, allowing the usage of a smaller vacuum padding region.

For an efficient implementation of PME, it is essential to optimally split the charge density into a smooth (low-frequency) component solved in the reciprocal space and a high-frequency residual handled in the real space. This decomposition enables the use of relatively coarse grids. Sophisticated smoothing and splitting schemes have been developed for this purpose,<sup>60</sup> but their details are beyond the scope of this article. Nevertheless, even with these optimizations (imposing PBCs on the system, using highly optimized PME solvers and FFT libraries), electrostatics still accounts for a relevant portion of the computational cost in classical molecular dynamics simulations.

Here, GridFF offers major advantages in both speed and accuracy. Since the electrostatic potential of the substrate is precomputed, the computational cost of solving for the electrostatic potential (via PME, or any other method) is removed entirely from the molecular dynamics (MD) run. In addition, periodic boundary conditions are imposed only on the substrate, and not artificially on the molecular system too. This means that the molecule does not actually interact with its periodic images. Moreover, in fully periodic systems (*e.g.*, a pristine surface), all interactions can be folded into the unit cell of the substrate, even if the molecular adsorbate is much larger, and therefore storing all interaction data in a minimal grid. During the MD run, the atomic coordinates of the adsorbate are then mapped into the surface unit cell and used for computing energies and forces. In addition, the surface potential becomes negligible just a few Å above the substrate, as both Morse and electrostatic components decay exponentially with the height. For example, the potential of a pristine NaCl substrate can be stored in as little as 32 Å<sup>3</sup> or 256 kB per component. For non-periodic systems (*e.g.*, point defects, step edges, AFM tips), the required memory footprint is significantly higher, *e.g.*, 100 cubic nanometers and 800 MB per compo-

nent in our largest supercell of 20×20. Overall, aside from the assumption of surface rigidity, the main limitation of GridFF is memory usage.

In the present work, we test the GridFF approach using a simplified electrostatic solver, which, unlike PME, omits the real-space residual entirely and relies solely on solving the Poisson equation  $\nabla^2 V = \rho$  in the reciprocal space. In this respect, our implementation more closely resembles the electrostatic solvers used in density functional theory codes (*e.g.*, SIESTA<sup>61</sup> or VASP<sup>62</sup>), than those based on classical force fields like LAMMPS. Besides simplicity, our motivation for this approach is the possibility to generate GridFF directly from *ab initio* charge densities without requiring atomic charge assignment or projection. Thanks to the relatively fine grid spacing (0.1 Å), this reciprocal-space-only solver achieves an accuracy of about 0.01 meV, which is sufficient for most purposes. Nevertheless, in future work, we plan to implement the full PME algorithm including the real-space correction to further improve accuracy.

## 5 Interpolation

Among the many numerical algorithms developed for function approximation and interpolation, we seek those that offer optimal performance on current computing hardware while maintaining sufficient accuracy. Additionally, we require methods that are completely general (*i.e.*, do not assume any particular functional form of the potential) and that can be used not only for pairwise interaction potentials, but also for potentials derived from electron densities. These requirements effectively constrain us to low-degree polynomial approximations defined on orthogonal uniform grids, which are also compatible with FFT algorithms used in long-range electrostatics.

A crucial consideration for high-performance implementation on modern CPUs and GPUs is the memory access pattern and cache locality. Contemporary hardware can perform hundreds of arithmetic operations (*e.g.*, additions or mul-

tuplications) in the time that it takes to read a single number from global memory. To mitigate this bottleneck, fast cache memory is used to pre-load data stored at nearby addresses. Thus, interpolation algorithms can be significantly accelerated when the data required to evaluate the potential at a given atomic position are collocated in memory and accessed in contiguous blocks.

In the original application of grid-projected potentials for AFM imaging (ppafm),<sup>45,63</sup> the trilinear interpolation was found sufficient, and even implemented in a hardware-accelerated form with reduced numerical precision. However, for simulations involving self-assembly or nanomanipulation of molecules on surfaces (especially under low-temperature conditions), a higher accuracy is required. Such systems can be sensitive to energy differences on the order of fractions of a meV, which can qualitatively affect trajectory bifurcations and final states.

Another fundamental problem of the trilinear interpolation approach is the inconsistency between interpolated forces and energy. In that implementation, the force components ( $F_x$ ,  $F_y$ ,  $F_z$ ) and energy  $E$  were stored and interpolated independently. This not only requires storing four times more data in memory ( $E$ ,  $F_x$ ,  $F_y$  and  $F_z$ , instead of just  $E$ ), but also implies that the resulting force is not the exact gradient of the energy field. This is because the derivative of a piecewise linear energy function is a piecewise constant function, while the interpolated forces are instead piecewise linear. This may cause difficulties to converge forces in molecular dynamics below a certain threshold, and/or for energy conservation.

To resolve this, we implemented a tricubic interpolation of the energy field, where forces are obtained analytically as the gradient of the piecewise cubic polynomials. In one dimension, this produces force profiles that are piecewise quadratic and therefore continuous and smooth. Formerly, we tested several approaches, including Hermite cubic polynomials, but ultimately selected cubic B-splines, which provided the best trade-off between interpolation accuracy and computational performance. Tricubic B-splines are also used in some ligand-docking ap-

plications, in cases where high quality forces are required, although typically with coarser grid spacing.<sup>51,64</sup>

The one-dimensional cubic B-spline interpolation on an interval  $(x_i, x_{i+1})$  can be expressed as a linear combination

$$f(x) = \sum_{j=-1}^2 B\left(\frac{x - x_{i+j}}{\Delta x}\right) b_{i+j} \quad (5)$$

of B-spline basis functions  $B(t)$  positioned at four points  $(x_{i-1}, x_i, x_{i+1}, x_{i+2})$  separated by a grid spacing  $\Delta x$ . The B-spline basis is a symmetric piecewise cubic polynomial defined as

$$B(t) = \begin{cases} \frac{2}{3} - t^2 + \frac{1}{2}|t|^3, & |t| < 1, \\ \frac{1}{6}(2 - |t|)^3, & 1 \leq |t| < 2, \\ 0, & |t| \geq 2. \end{cases} \quad (6)$$

The 3D cubic B-spline interpolation is implemented as a Cartesian (tensor) product of 1D interpolations. This means that each evaluation accesses data from a  $4 \times 4 \times 4$  block of the nearest grid points – namely, 64 values in total. For each potential component (*i.e.*, Coulomb, Pauli, and London), this corresponds to reading 192 floating-point numbers.

The grid is stored in memory such that the fastest-changing axis (typically  $z$ ) is laid out contiguously, so blocks of four values along  $z$  are collocated in memory. Although the full interpolation could be evaluated as a direct sum over 64 basis functions weighted by precomputed coefficients, more efficient implementations – like ours – decompose the operation into a sequence of 1D interpolations. Specifically, we perform 16 1D interpolations along  $z$ , followed by 4 along  $y$ , and finally 1 along  $x$ . Starting with the fastest axis ( $z$  in our case) ensures optimal cache locality and allows the use of single-instruction-multiple-data vectorization.

According to our benchmarks, this tricubic B-spline interpolation is only about two times slower than a trilinear interpolation (using grids for  $E$ ,  $F_x$ ,  $F_y$  and  $F_z$ ), while providing several orders of magnitude higher accuracy. Moreover, in practical simulations, the cost of evaluating molecule-substrate interactions (using either interpolation scheme) is anyway about one hun-

dred times faster (on CPU) than the cost of evaluating molecule-molecule pairwise interactions – even for small systems ( $\sim 50$  atoms). Therefore, the additional cost of the tricubic interpolation is negligible in real workloads. On GPU, the GridFF interpolation consumes a significantly higher share of performance budget (see Section 6) as the GPU performance is limited by global memory access rather than arithmetic operations.

One complication of using B-splines is that the expansion coefficients  $b_i$ , stored at each grid point, are not known *a priori*. They must be fitted such that the interpolated potential reproduces the reference values at grid nodes. While this fitting is a linear problem involving a very sparse matrix, the problem size is large: for typical grid spacing ( $\sim 0.1$  Å), a cubic nanometer contains on the order of  $10^6$  grid points. This makes iterative solvers more feasible than direct matrix inversion approaches.

Currently, we use a simple gradient descent algorithm to minimize the root mean square error across all grid points. Although this method is not particularly efficient and may require thousands of iterations to reach convergence at the desired accuracy, we do not consider this as a bottleneck. In a typical workflow, the grid is precomputed once for a given substrate, and then reused in many simulations. Therefore, we have not prioritized further optimizations of the coefficient fitting procedure.

## 6 Accuracy and performance tests on CPU

In order to benchmark the accuracy of the proposed approach, we performed several systematic tests calculations using GridFF as implemented in FireCore<sup>37</sup> and all-atom simulations using the LAMMPS package.<sup>35</sup> The studied system is the desorption and manipulation of a 3,4,9,10-perylenetetracarboxylic dianhydride (PTCDA) molecule on top of a NaCl slab. This system was chosen as it has been extensively studied experimentally by means of SPM techniques.<sup>65–67</sup> Also robotic manipulation of the PTCDA molecule (although on metallic sub-

strate) originally motivated our work.<sup>20</sup>

First, we performed rigid (*i.e.*, with fixed relative positions of the atoms in the molecule) vertical and lateral scans of PTCDA on a  $8 \times 8 \times 3$  NaCl(001) surface slab to compare individual potential components between GridFF and LAMMPS. Next, we conducted relaxed scans with the same molecular and substrate configurations, allowing the system to undergo molecular relaxation, therefore more closely mimicking a manipulation experiment with AFM. After validating the relaxed potential behavior, we extended our tests to include defective substrates. We introduced a neutral, nearly isolated defect by removing 2 atoms from the surface of a  $20 \times 20 \times 3$  NaCl supercell, equivalent to a defect density of approximately 0.08%. Using the same PTCDA molecule, we performed lateral scans across this defected surface to test the capability of the method to handle surface irregularities. Finally, we compared the performance of GridFF and all-atom calculations for increasing substrate sizes ranging from  $8 \times 8 \times 3$  to  $20 \times 20 \times 3$  supercells.

The molecular structure of PTCDA was retrieved from a previous work of one of us on high resolution AFM imaging,<sup>45</sup> and supplemented with atomic charges determined using the restrained electrostatic potential fitting scheme.<sup>68</sup> The NaCl substrate was modeled by three *fcc* atomic layers with lattice spacing of 4.0 Å, and charges for the Na/Cl ions set to  $\pm 0.9e$  according to the Bader analysis.<sup>69</sup> The intramolecular interactions are modeled using the universal force field (UFF)<sup>70</sup> both in FireCore and LAMMPS. UFF values were also used to obtain the Morse parameters modeling the molecule-substrate interaction (the value of the  $\alpha$  parameter was set to  $1.5 \text{ Å}^{-1}$  for all pairs, and a cutoff of 17 Å was applied).

Within the GridFF framework, we generated potential energy grids for the NaCl(001) substrate using a fine grid spacing of 0.1 Å and setting the maximum iterations to 3000 for the generation of the B-spline parameters, achieving fitting errors on the order of  $10^{-5}$  for both Morse and Coulomb potentials. For the treatment of the slowly decaying electrostatic interactions, in FireCore we used a reciprocal-space

Poisson solver as reported above, whilst in LAMMPS they were evaluated with the closely related particle-particle particle-mesh (PPPM) method<sup>71</sup> with a real space cutoff of 15 Å. The relative accuracy of reciprocal part of PPPM kernel was set to  $10^{-8}$  in rigid scans to obtain high-accuracy reference energy profiles. Such a stringent tolerance was necessary since a more standard setting ( $10^{-6}$ ) produced numerical artifacts in LAMMPS calculations larger than the error coming from the reciprocal-space-only Poisson solver in GridFF. Nevertheless, a more relaxed threshold of  $10^{-6}$  was chosen for relaxed scans with LAMMPS, as these simulations were also used for benchmarking the performance in typical use-cases. Therefore we should note that in case of relaxed scans FireCore simulations are actually more accurate than LAMMPS results, while being significantly faster. To ensure a fair comparison, both FireCore and LAMMPS used the same FIRE algorithm<sup>72</sup> for the structural optimization with a convergence threshold for forces of  $10^{-3}$  eV/Å.

## 6.1 Rigid scans of PTCDA on NaCl

The profiles in Figure 1 show the contributions to the energy variations when a PTCDA molecule is rigidly moved away from the NaCl surface. The decomposition of the total interaction potential into individual components ensures that the underlying interaction physics is accurately reproduced by the GridFF approach. The Morse potential component (red) describes the short-range interactions (encompassing both Pauli repulsion and van der Waals attraction), whilst the Coulomb potential component (blue) captures the long-range electrostatics between the PTCDA molecular charge distribution and the ionic NaCl substrate. The total potential energy curve (green) represents the superposition of all interaction components, yielding an equilibrium adsorption configuration at  $Z = 3.1$  Å with a total binding energy of -0.89 eV. All energy profiles overlap perfectly, and therefore, to quantitatively estimate the accuracy of GridFF approach, we also report the energy differences between the

two methods on the right  $y$ -axis. In all cases, the agreement is remarkable (considering the fitting error in the interpolation procedure, and the PPPM accuracy set in the LAMMPS calculations), with the Morse potential component exhibiting differences on the order of  $10^{-6}$  eV, whilst the Coulomb component shows discrepancies of approximately  $10^{-5}$  eV. Overall, the differences are dominated by the electrostatics contribution, due to the plane-wave cut-off of the reciprocal Poisson solver and the aforementioned omission of real-space residual from PME employed in the GridFF calculations. In both cases, the differences tend to increase at small separation distances (where the slope of the profiles is maximal in absolute values).

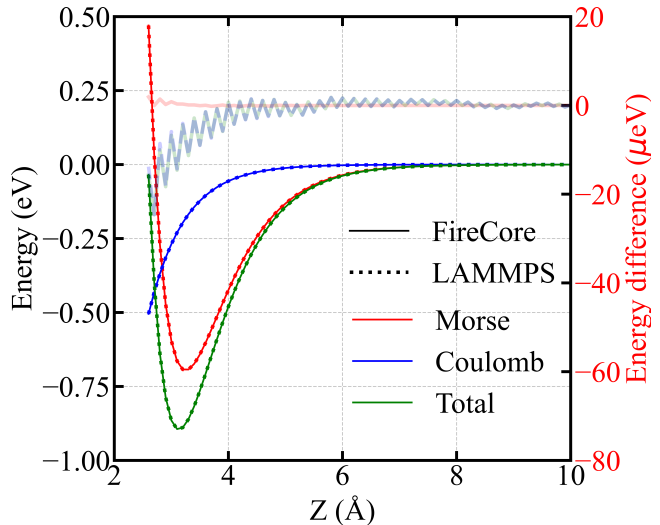


Figure 1: Energy profiles for a PTCDA molecule interacting with a NaCl surface as a function of the separation distance along the  $z$ -direction. The total potential is decomposed into Morse (red) and Coulomb (blue) components, with the total energy (green) shown for the sake of completeness. Calculations using the GridFF approach as implemented in the FireCore code are reported with thin solid lines, whilst all-atom simulations from LAMMPS are in thick dashed lines. The energy differences between the two methods are plotted with semi-transparent lines and with the same color scheme.

Next, we performed lateral two-dimensional rigid scans on the  $xy$ -plane by rigidly displacing the PTCDA molecule with a step length of

0.1 Å and at a constant height of 3.3 Å from the surface. Figure 2 shows the total interaction energy as a function of the in-plane position of the molecule across one unit cell of the NaCl(001) substrate. Such a 2D scan provides information about the preferred adsorption sites and barriers for lateral diffusion or manipulation of the molecule on the surface. The left and center panels show the PES calculated by FireCore and the reference LAMMPS force field, respectively. Both methods produce a qualitatively identical energy landscape, with an energy barrier of 0.46 eV located at the center of the unit cell. The right panel displays the absolute energy difference between the FireCore and LAMMPS calculations. As in the previous case, the absolute error is on the order of  $10^{-5}$  eV. In summary, these results demonstrate that FireCore accurately reproduces the whole interaction energy landscape.

## 6.2 Relaxed detachment of PTCDA from NaCl

In order to simulate more realistically the manipulation of PTCDA with an SPM tip on a surface at low temperature, we performed calculations where we restrained the position of one atom (a carboxylic oxygen at the corner) of the molecule and let the position of the other atoms relax. In the first set of simulations, at each step we displaced the  $z$ -component of the position of the selected atom by 0.1 Å, starting from 1.3 to 20 Å above the NaCl(001) surface. Such a computational setup effectively mimics the experimental protocols where a functionalized tip is used to grasp and manipulate individual molecules on surfaces by forming a mechanical contact with a specific atomic site.<sup>19,20</sup> The resulting relaxed potential energy curve reported in Figure 3 exhibits significantly different characteristics compared to the rigid scan. The global minimum occurs at approximately  $Z = 2.8$  Å with a binding energy of -0.94 eV, representing the equilibrium adsorption configuration. The larger binding energy (compared to the rigid scan) demonstrates the importance of molecular flexibility in achieving optimal molecule-surface interactions through

conformational adaptation. The unbinding energy profile is also qualitatively different, presenting multiple local minima and discontinuities, particularly in the intermediate separation range (6-15 Å). These features arise from the interplay between attractive molecule-surface interactions and internal molecular strain. The molecular relaxation allows for rotation, tilting, and conformational changes (that can create metastable adsorption states not accessible in rigid scan calculations), and eventually leading to the sudden detachment of the molecule from the substrate. As already pointed out, in the proximity of the sudden changes of molecular orientation/conformation, the relaxation dynamics is more sensitive to small force differences, leading to bifurcation in the taken path. Nevertheless, also in this case the quantitative agreement between FireCore and LAMMPS is good, with energy differences remaining below 0.9 meV across the entire scan range. These results validate the ability of the GridFF approach to accurately capture the energetics and the structural response of a molecule under mechanical manipulation, a critical requirement for predicting AFM-based molecular device fabrication and single-molecule manipulation protocols.

## 6.3 Dragging the PTCDA molecule over a defect

The goal of this set of simulations is to mimic the dragging of a PTCDA molecule by a SPM molecule over a NaCl surface along the diagonal of the substrate cell. As done before, this was achieved by fixing the position of one atom of the PTCDA molecule (marked by the red dot in Figure 4), and systematically displacing it along the scan direction while allowing the entire molecular system to relax at each step. We have considered a 20x20x3 NaCl substrate with 2400 atoms for the pristine surface, and a system with a neutral defect (*i.e.*, by removing one Na and one Cl atoms next to each other from the topmost atomic layer) placed at the center of the cell.

The top panels of Figure 4 illustrate the sliding behavior on a defect-free NaCl surface. The

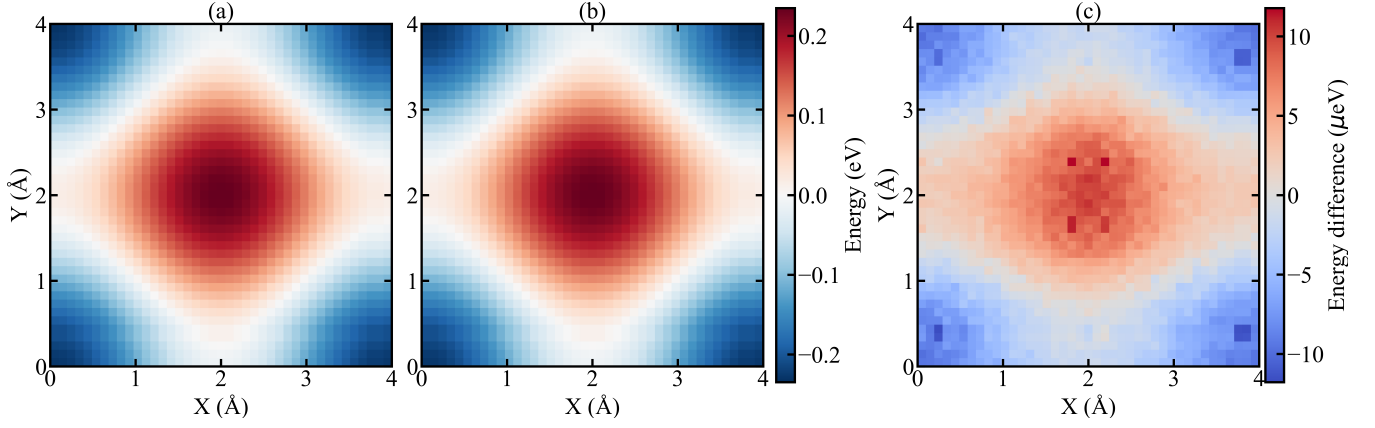


Figure 2: Rigid PES of a PTCDA molecule interacting with a NaCl surface at a separation height of 3.3 Å, obtained with the GridFF approach as implemented in the FireCore (a), and all-atom calculations from LAMMPS (b). Panel (c) reports the energy difference between FireCore and LAMMPS.

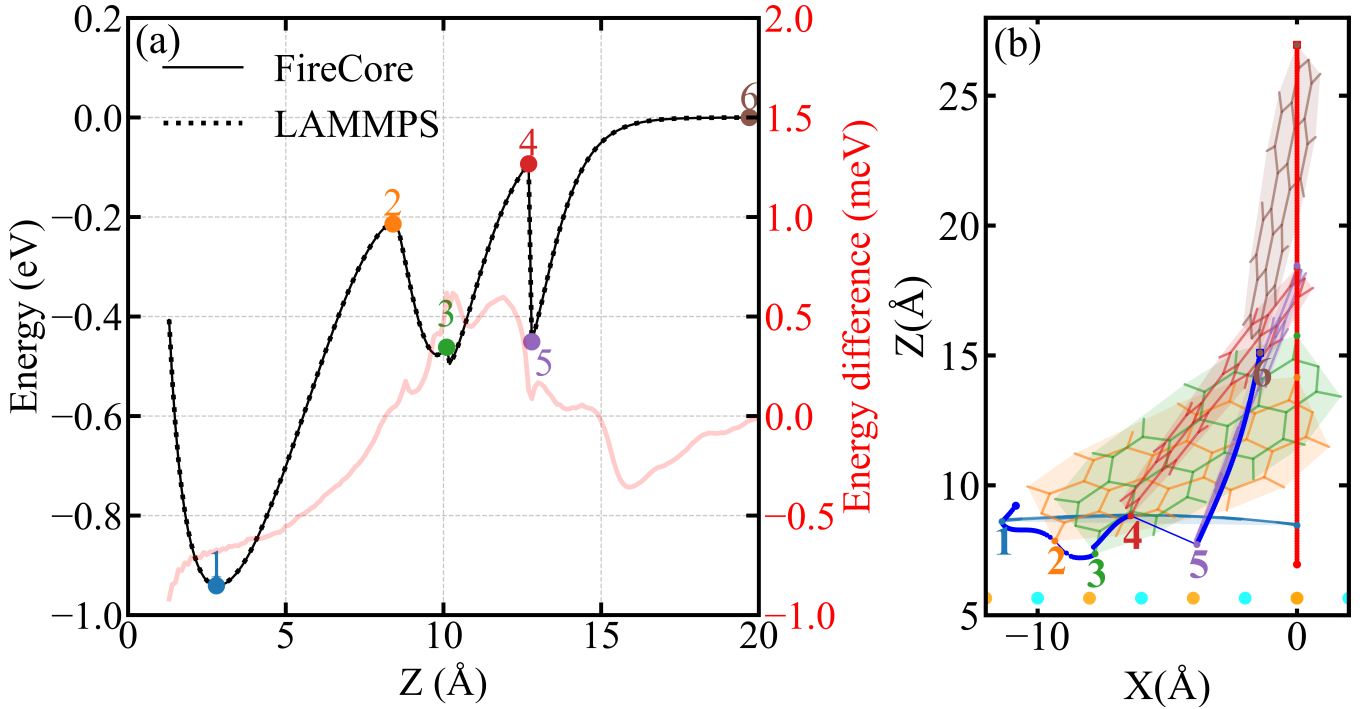


Figure 3: (a) Energy profiles for both GridFF (FireCore) and all-atom (LAMMPS) calculation, and (b) selected configurations of a PTCDA molecule lifted up from a NaCl surface. In panel (b), the red and blue dots represent the atom that is displaced vertically during the scan, and the carbonyl oxygen at the opposite position of the PTCDA molecule, respectively. The six molecular configurations shown in (b) correspond to the marked dots in (a). Na and Cl ions are depicted in orange and cyan, respectively (only the topmost layer is shown).

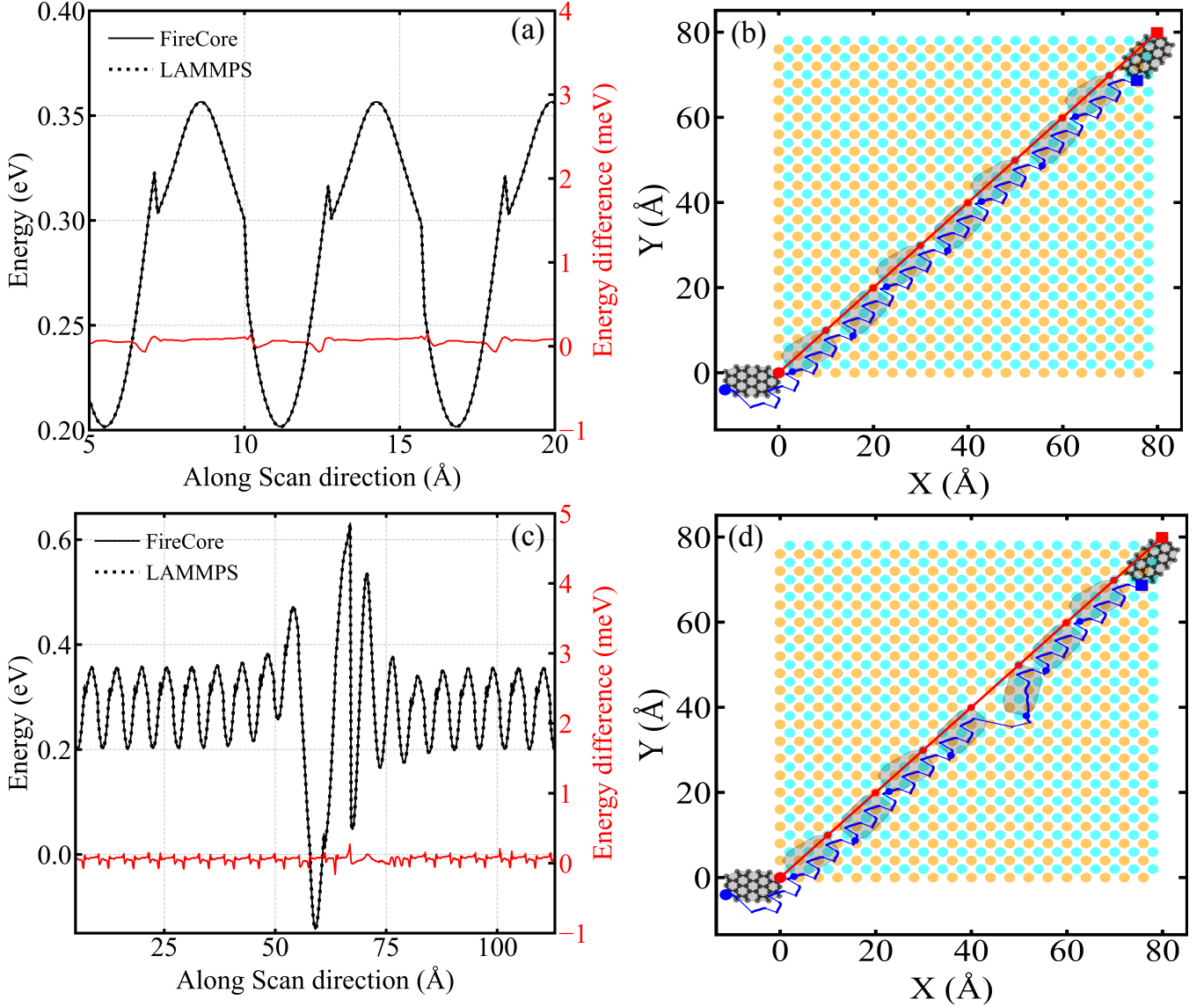


Figure 4: Comparison between GridFF (Firecore) and all-atom (LAMMPS) calculations for a PTCDA molecule dragged over a NaCl surface with and without the presence of a defect. (a) Energy profile and (b) the corresponding set of relaxed configurations on a pristine 20x20x3 NaCl substrate. (c) Energy profile and (d) the corresponding set of relaxed configurations on the same substrate in the presence of an isolated neutral defect at the center of the cell. In the energy plots (a, c), the potentials calculated by FireCore (dashed orange) and LAMMPS (solid blue) are shown on the left axis, with their absolute difference (red) on the right axis. In the trajectory plots (b, d), the path of the restrained atom (red) and of the atom in the opposite corner of the molecule (blue) are shown with dots, illustrating the path taken by the molecule over the Na (orange) and Cl (cyan) ions of the top substrate layer.



energy profile in Figure 4a shows a quantitative agreement between FireCore and LAMMPS, with the difference remaining consistently below 0.9 meV. The energy minima correspond to the PTCDA molecule settling into energetically favorable adsorption sites that align with the underlying Na and Cl ion lattice. The energy maxima represent the potential barriers that the molecule must overcome to move between these stable sites. The non-smooth nature of the energy profile arises from the interplay between the static interaction field generated by the substrate and the orientational and conformational degrees of freedom of the PTCDA molecule. As it is pulled across the surface, the molecule continuously adjusts its orientation and internal geometry to minimize the total energy, leading to the characteristic ‘stick-slip’ motion (reminiscent of different systems studied by AFM experiments and MD simulations<sup>73,74</sup>) visually depicted in the trajectory plot (Figure 4b). The path of the unconstrained opposite corner atom (blue dot) clearly deviates from the straight-line path of the fixed atom, hopping between adjacent lattice sites.

The bottom panels of Figure 4 shows the capability of FireCore to handle localized and chemically complex features, such as a neutral point defect in the substrate. It can be observed from the graph that, far from the defect, the energy profile in Figure 4c retains the periodic corrugation of the pristine surface. However, as the molecule approaches the defect location (at the mid-point of the scan length), the energy profile changes drastically. A sharp, deep potential well emerges, indicating a strong pinning of the molecule to the defect site. This interaction is significantly stronger than the regular surface corrugation, with an energy stabilization of over 0.77 eV. Figure 4d provides an intuitive real-space visualization of this event: the path taken by the molecule shows a lateral deviation as it is influenced by the presence of the defect. The PTCDA molecule reorients itself to maximize its favorable interaction with the defect before being pulled away, which requires overcoming a substantial energy barrier. Also in this case, the energy profile obtained with GridFF perfectly matches the one from reference calculations,

with maximum deviations in the order of 0.9 meV. Overall, this demonstrates the capability of the proposed approach to accurately model the molecule-surface interaction even in the presence of more complicated features such as a point defect, making it a powerful tool for predictive materials simulation.

## 6.4 Performance comparison

The lateral relaxed scan on the pristine surface described in the previous section was also used to benchmark the performance of the CPU implementation of GridFF in FireCore with respect to LAMMPS. The dynamical relaxation with the FIRE algorithm<sup>72</sup> is a good choice for such comparison, as the overheads (*e.g.*, setup and initialization of the system) are amortized over the thousands of steps required for the structure relaxation. To ensure a reliable comparison between the two approaches, and avoid any dependence on the details of the relaxation algorithm, the number of relaxation steps was set to the same value (5000), and with a tiny threshold on the force convergence criterion to ensure that the maximum number of relaxation steps is always reached. In this way we can directly compare the calculation walltimes needed to complete the dragging path, as in both cases the same number of relaxation steps (and therefore of force and energy evaluations) are performed. It must be stressed that, in order to have a fair comparison, the PPPM accuracy tolerance in LAMMPS was increased to  $10^{-6}$  (with respect to  $10^{-8}$  used for rigid-scan calculations). Moreover, again for the sake of fairness, we performed calculations also directly excluding the computation of pairwise interactions within the substrate, by removing the appropriate atoms from the neighbor lists.

Figure 5 shows the comparison of the computational performance between LAMMPS and Firecore, together with the scaling with respect to the system size (ranging from  $8\times 8$  to  $20\times 20$  NaCl unit cells, corresponding to 384 to 2400 substrate atoms). All calculations were performed on the same computer equipped with an AMD EPYC 7513 CPU (2.6 GHz) using a single core. Firecore achieves good speedup factors

ranging from  $113\times$  for the smallest system to  $751\times$  for the largest, reducing execution times from hours to minutes, as also shown in Table 1. Notably, the largest system, that requires over 45 hours in LAMMPS, completes in less than 4 minutes with Firecore. Moreover, as one can notice from the different slopes in Figure 5, GridFF shows also a superior scaling behavior with respect to the system size, if compared to all-atom calculations. In fact, by moving from the smallest to the largest systems, the total number of atoms increases by about 6 times. Correspondingly, the execution time (normalized by the total number of path points) increases by almost 8 times in LAMMPS, while in FireCore the increment is only about 20 %. Such dependence of speedup factors on the system size indicate that the algorithmic advantages of GridFF may become even more pronounced for larger systems (such as pulling of graphene ribbons<sup>3</sup> or DNA), enabling practical high-throughput screening and statistical sampling for several applications.

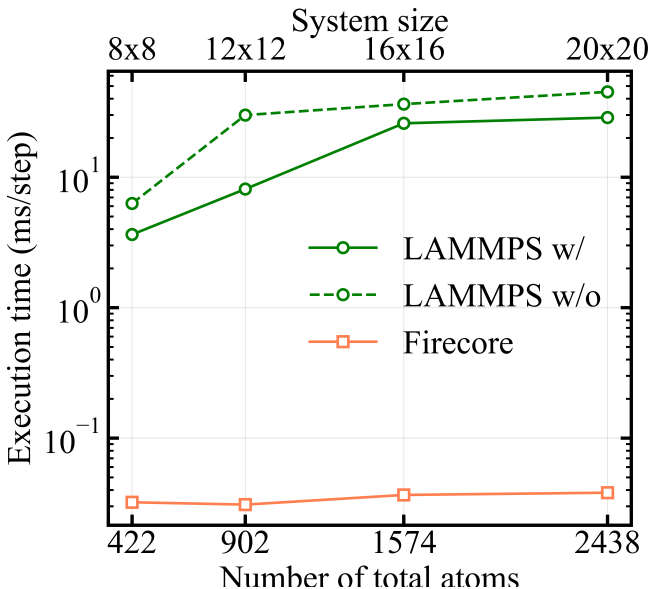


Figure 5: Execution walltimes for FireCore and LAMMPS as a function of the system size. The green solid and dashed lines represent LAMMPS calculations with and without excluding the computation of pairwise interactions within the substrate atoms, respectively.

## 7 Configuration sampling on GPU

While the simulations of dragging of the PTCDA molecule using CPU allows a side-by-side comparison of the accuracy and performance of GridFF/FireCore with LAMMPS, the main strength of our approach lies in its ability to accelerate the exploration of large configuration spaces of flexible molecules on surfaces. This includes tasks such as finding the most stable binding configuration (*i.e.*, the global energy minimum in the configuration space, which is a hard problem), or computing the binding potential of mean force, which requires sampling all energetically relevant configurations.

To illustrate the performance of FireCore in such applications, we conducted a case study of the adsorption of a xylitol molecule on a sodium chloride surface with a single chlorine vacancy. The presence of five hydroxyl groups in the xylitol molecule creates numerous possibilities for hydrogen bonding with the ionic surface. Combined with molecular flexibility due to free rotations around sigma bonds, this results in a complex energy landscape characterized by many local minima.

To comprehensively explore this vast conformational space, we employed a minima hopping technique adapted for surface adsorption. This method systematically samples different configurations by perturbing the molecular structure (*i.e.*, by performing 1000 steps of Langevin molecular dynamics at a relatively high temperature of 300 K, followed by dynamical relaxation to the nearest local minimum. Each energy minimization was carried out until forces converged below  $0.1 \text{ meV}/\text{\AA}$ , ensuring an accurate representation of the stable configuration.

Efficient implementation of molecular dynamics for small molecules like this on GPU faces several challenges. Modern GPUs are equipped with thousands of cores, which is significantly more than the number of atoms in such systems (typically 50-100 atoms; rigid substrate atoms represented by GridFF are excluded). Although parallelization over individual pair-

Table 1: Execution times and computational speedups for FireCore and LAMMPS for different system sizes.

System size	Total steps	Firecore Time (s)	LAMMPS			
			with exclusion		without exclusion	
			Time (s)	Speedup	Time (s)	Speedup
8x8	2265000	73	8240	113	14256	195
12x12	3395000	105	27549	262	101655	968
16x16	4525000	166	117259	706	164526	991
20x20	5660000	216	162257	751	255390	1182

wise interactions (rather than atoms) is possible, synchronized output of forces (*i.e.*, reduction) from different threads to global memory would require thread synchronization, reducing performance. We address this challenge by simulating multiple replicas of the same system in parallel. Testing showed that the optimal performance is achieved with  $\sim 5000$  replicas, in the case of the xylitol molecule. Moreover, the time required to evaluate forces (*i.e.*, summing over all bonding and non-covalent interactions) for such small systems is often shorter than the time required to transfer atomic coordinates (and forces) to and from the GPU. Therefore, the entire molecular dynamics loop – including force evaluation and integration of the equations of motion – must be executed entirely on the GPU, eliminating the need for costly synchronization with the CPU.

While Langevin dynamics is performed fully on the GPU and downloaded only every few hundred steps for visualization, the dynamical relaxation requires global properties which involve reductions over all atoms – *i.e.*, thread synchronization. In particular, for dynamical relaxations, one needs to calculate the norm of the whole force vector  $\vec{F}$  in order to check the force convergence criterion, and to set to zero all velocities ( $\vec{v} = 0$ ) if the system inertially moves up the hill ( $\langle \vec{F} | \vec{v} \rangle < 0$ ). To handle this, we download the system state every 100 steps and perform these operations on the CPU (although in principle, such reductions could also be performed on the GPU but at the cost of more complicated kernels). At any rate, not performing the check at every step does not seem to significantly hamper the overall perfor-

mance of the algorithm. We attribute this to the smoothness of the trajectory near the minimum (which often is a long narrow “valley”) and to the fact that a relaxation typically takes several thousand steps anyway.

To identify unique structures, each optimized geometry is compared with all previously minimized structures using a root-mean-square deviation criterion (with a threshold of 0.1 Å), accounting for both conformational differences and variations in adsorption site and orientation relative to the surface. For this purpose, geometries are downloaded from the GPU and the comparison is performed on the CPU, typically only once per several thousand steps. Although the computational cost of comparison with hundreds or thousands of previously found local minima is substantial (using only CPU), it is amortized in the dominating cost of thermalization and relaxation, and therefore we did not attempt to implement this sub-task on GPU yet.

The simulation can be run either as a batch calculation via the FireCore Python API – suitable for supercomputer production runs – or through a graphical user interface (GUI), useful for debugging and educational purposes on desktop computers. Figure 6a shows a screenshot from such an interactive simulation, highlighting a selected configuration near the vacancy, while the other replicas are shown as transparent skeletons in the background.

In Figure 6b,c we present performance metrics for this simulation using both the GridFF approach and a naive all-atom FireCore GPU MD-loop implementation. In the all-atom simulation, molecule-substrate interactions are computed as a direct sum of pairwise interac-

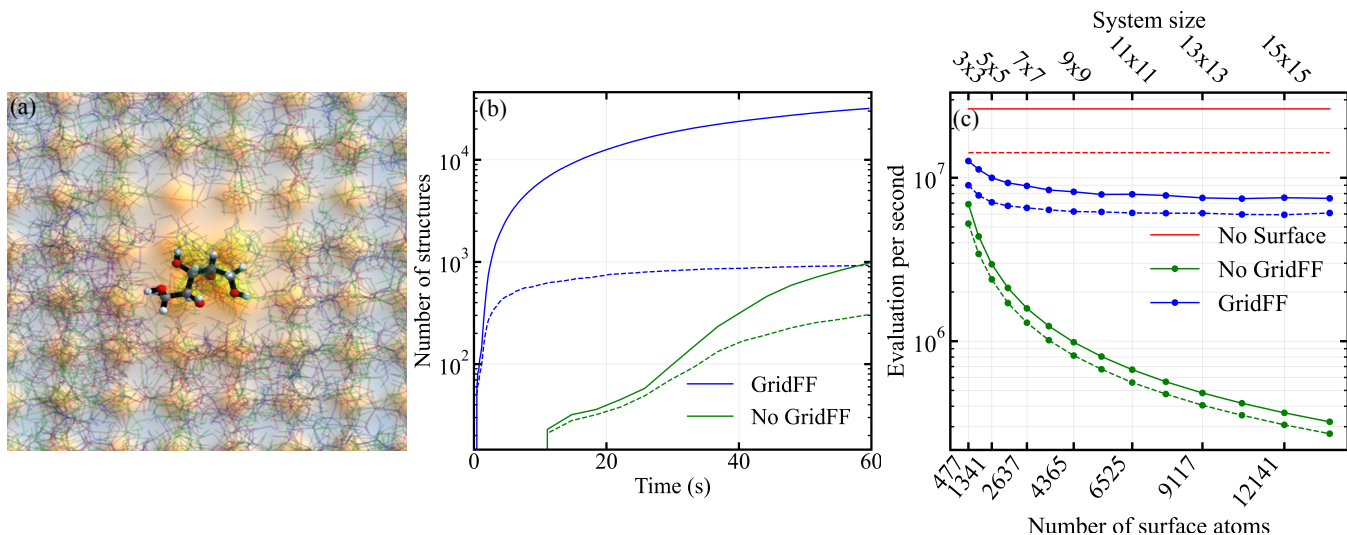


Figure 6: Analysis of xylitol adsorption on NaCl using GridFF. (a) Visualization of a 2000-replica simulation of representative xylitol molecule configurations adsorbed on the NaCl(001) surface with a Cl-hole. (b) Number of total (solid) and unique (dashed) structures found in a short run using FireCore. Blue and green lines represent the outcomes of simulations done on  $16 \times 16 \times 3$  surface with a Cl-hole using the GridFF and standard all-atom approaches, respectively. (c) Number of MD steps per second using GridFF (blue) and all-atom (green) calculations, and for an isolated xylitol molecule (red) for reference, as a function of the system size. Solid and dashed lines corresponds to calculations with different settings.

tions (*i.e.*, without Ewald summation as used in LAMMPS). These are summed over the nearest periodic images of the surface supercell, while the interactions between surface atoms are omitted. Figure 6c reports the total number of substrate atoms interacting with the molecule (*i.e.*, the number of atoms in the supercell plus its 9 periodic images used for the direct-sum evaluation). Notably, GridFF-based calculations are not only significantly faster but also more accurate, owing to the use of Ewald summation in constructing the GridFF.

Figure 6b presents a quantitative analysis of the sampling efficiency, showing the number of converged and unique structures found as a function of the execution time. The number of converged structures increases proportionally with the number of attempts, indicating the consistent performance of the energy minimization protocol. In contrast, the number of unique structures rises rapidly at early times and plateaus around 800 structures, despite continued sampling. This saturation suggests that our approach exhaustively explored the relevant conformational space of the xylitol-

NaCl system under the chosen computational model.

Looking closely at Figure 6b, we observe that, in the all-atom simulation, the first batch of structures is found only after  $\sim 10$  seconds, reflecting the time required for the initial thermalization. This synchronization delay also explains why the green curve deviates from a steady-state sampling behavior around 20 seconds after the simulation start. A similar behavior is seen in the GridFF simulation, but it is compressed into the first 1-2 seconds due to its  $\sim 20\times$  higher performance.

Figure 6c provides a systematic analysis of how performance scales with system size. GridFF shows clear performance superiority for larger supercells, achieving a throughput of approximately 7.5 million MD steps per second for the largest systems, compared to only 0.3 million steps per second for the all-atom approach. Notably, GridFF performance remains stable regardless of the system size, while the all-atom approach degrades steadily with system size, making the performance advantage of GridFF even more pronounced for larger sys-

tems.

For small supercells (<200 atoms in the supercell, <1800 atoms in 9 images), GridFF shows a slight increase in performance, likely due to an improved cache efficiency as neighboring voxel memory addresses are more contiguous. This effect could potentially be exploited further by using coarser grids.

## 8 FireCore from the user perspective

FireCore is written in C++ and OpenCL languages, with python binding providing a convenient scripting interface. The generation of the surface potential can be done internally on CPU, or using a standalone pyOpenCL accelerated python script, which takes the structure of the substrate (provided by the user in the `xyz` or `mol` format), and the desired voxel size for the grid, and it generates and stores the grid potential. The syntax for generating the grid potentials presented in this paper is:

```
python3 generate_grid.py
```

The main simulation engine of FireCore can perform energy optimization or molecular dynamics calculations of molecules on surfaces. To start a run, is sufficient to provide the geometries of the molecule and the substrate. Supported formats are `xyz` and `mol`. In the case that a plain `xyz` file is provided for the molecule, FireCore automatically detect the bonding topology. FireCore accordingly assigns the atomic types and all parameters needed for bonded and non-bonded interactions. Currently are available only UFF and sp3FF (our home brew potential which was not yet published). The user can also directly customize the parameter files for bonded and non-bonded interactions. Next, the user can decide whether to run grid-based or all-atom simulations. A folder (which also contains a `README` file with commands and explanations) with all files needed to run the examples reported in this paper is available in the FireCore repository.<sup>75</sup> To reproduce the calculations presented in Section 6, one can run the following command:

```
python3 generate_scans.py
```

Along with the command line interface, FireCore also provides a GUI for running interactive simulations, real-time visualization of structural relaxations and molecular dynamics runs, including the multiple-replica feature described in Section 7. The GUI allows the user to visualize atomic types, charges, and electrostatic potentials. It also enables the interactive manipulation of molecules by picking and dragging atoms with the mouse (resembling what is done in AFM manipulation of molecules). The GUI can be run using the command:

```
bash FireCore/tests/tMolGUIapp/run.sh
```

Beside the above-mentioned functionalities, FireCore also implements other advanced features like the charge equilibration scheme,<sup>76</sup> a workflow for fitting hydrogen bond corrections from reference data (currently under development), the thermodynamic integration method for the calculation of free energy differences, and a QM/MM framework with an interface to the Fireball DFT(B) package<sup>77,78</sup> and integrated high-resolution AFM simulations.

## 9 Conclusions and Outlook

In this work, we have demonstrated that grid-projected force fields – originally inspired by methods used for ligand docking in molecular biology – can be successfully applied to surface science, particularly for simulating molecular adsorption and manipulation on surfaces using scanning probe microscopy at low temperatures. As implemented in the new open-source simulation package FireCore, the method achieves a speedup of 2-3 orders of magnitude (compared to conventional all-atom simulations) for a PTCDA molecule on a NaCl surface using a single CPU, while maintaining a high accuracy of the results. We further showcase the CPU and GPU implementations of the method in FireCore which enables sampling of millions of molecular configurations per second, making it possible to exhaustively explore all local minima of small flexible molecules (*e.g.*,

xylitol) within just a few minutes on a standard desktop GPU.

The main limitation of the method is the assumption of a rigid substrate. However, this is a common approximation even in traditional all-atom simulations, particularly due to the lack of accurate force fields for ionic crystal surfaces. This limitation can be partially mitigated by adjusting force field parameters to emulate the effective (softened) potential resulting from substrate atom deflections – a strategy commonly employed in ligand docking.<sup>54</sup> In a future work, we aim to address this limitation more rigorously by incorporating additional force field components that allow for local polarization and substrate deflection, based on linear response theory.<sup>79–81</sup> We are also developing a hydrogen-bond correction scheme within the GridFF framework, as well as density-derived potentials such as FDBM,<sup>44</sup> which promise to deliver accuracy far beyond traditional pairwise interactions, like Coulomb, Morse, or Lennard-Jones, while retaining unparalleled computational performance. Although in this study we opted for a conservative approach to GridFF interpolation using cubic B-splines with very fine grid spacing, we recognize opportunities to further optimize the memory footprint and potentially improve the speed via a better cache locality. This could be achieved by experimenting with alternative interpolation strategies, including power-transformed interpolations,<sup>52</sup> different forms of potential factorization, or non-uniform grid spacing schemes.<sup>82</sup>

**Acknowledgement** The authors thank Mithun Manikandan for the RESP calculations. This work was supported by the Czech Science Foundation, Project 22-06008M, and co-funded by the European Union (Physics for Future – Grant Agreement No. 101081515). A part of the computational resources was provided by the e-INFRA CZ project (ID:90254), supported by the Ministry of Education, Youth and Sports of the Czech Republic.

## References

- (1) Krim, J. Friction and energy dissipation mechanisms in adsorbed molecules and molecularly thin films. *Advances in Physics* **2012**, *61*, 155–323.
- (2) Villa, N. S.; Bonoldi, L.; Assanelli, G.; Notari, M.; Lucotti, A.; Tommasini, M.; Cuppen, H. M.; Galimberti, D. R. Digging into the friction reduction mechanism of organic friction modifiers on steel surfaces: Chains packing vs. molecule–metal interactions. *Tribology International* **2024**, *195*, 109649.
- (3) Kawai, S.; Benassi, A.; Gnecco, E.; Söde, H.; Pawlak, R.; Feng, X.; Müllen, K.; Passerone, D.; Pignedoli, C. A.; Ruffieux, P.; Fasel, R.; Meyer, E. Superlubricity of graphene nanoribbons on gold surfaces. *Science* **2016**, *351*, 957–961.
- (4) Chen, H.; Stoddart, J. F. From molecular to supramolecular electronics. *Nature Reviews Materials* **2021**, *6*, 804–828.
- (5) Surin, M.; Leclère, P.; De Feyter, S.; Abdel-Mottaleb, M. M. S.; De Schryver, F. C.; Henze, O.; Feast, W. J.; Lazzaroni, R. Molecule–Molecule versus Molecule–Substrate Interactions in the Assembly of Oligothiophenes at Surfaces. *The Journal of Physical Chemistry B* **2006**, *110*, 7898–7908.
- (6) Hieulle, J.; Stecker, C.; Ohmann, R.; Ono, L. K.; Qi, Y. Scanning Probe Microscopy Applied to Organic–Inorganic Halide Perovskite Materials and Solar Cells. *Small Methods* **2018**, *2*, 1700295.
- (7) Heimel, G.; Romaner, L.; Zojer, E.; Bredas, J.-L. The Interface Energetics of Self-Assembled Monolayers on Metals. *Accounts of Chemical Research* **2008**, *41*, 721–729.
- (8) Feng, X.; Peng, X.; Peng, B.; Li, Z.; Huang, W.; Yang, S.; Pei, K.; Sun, Z.;

- Huang, F.; Li, H.; Shuai, Z.; Zhai, T. Effect of Strong Intermolecular Interaction in 2D Inorganic Molecular Crystals. *Journal of the American Chemical Society* **2021**, *143*, 20192–20201.
- (9) Zhu, Y.; Yan, Y.; Feng, Y.; Liu, Y.; Lin, C.-Y.; Ai, Q.; Zhai, T.; Shin, B.; Xu, R.; Shen, H.; Fang, Q.; Zhang, X.; Bhagwandin, D.; Han, Y.; Zhu, H.; Glavin, N. R.; Ajayan, P. M.; Li, Q.; Lou, J. A General Synthesis Method for Covalent Organic Framework and Inorganic 2D Materials Hybrids. *Precision Chemistry* **2024**, *2*, 398–405.
- (10) George, S. M.; Yoon, B.; Dameron, A. A. Surface Chemistry for Molecular Layer Deposition of Organic and Hybrid Organic–Inorganic Polymers. *Accounts of Chemical Research* **2009**, *42*, 498–508.
- (11) Yuan, M.; Qiu, Y.; Gao, H.; Feng, J.; Jiang, L.; Wu, Y. Molecular Electronics: From Nanostructure Assembly to Device Integration. *Journal of the American Chemical Society* **2024**, *146*, 7885–7904.
- (12) Shi, Y.-L.; Wang, X.-D. 1D Organic Micro/Nanostructures for Photonics. *Advanced Functional Materials* **2021**, *31*, 2008149.
- (13) Chen, H.; Zhao, L. Quantum-dot cellular automata as a potential technology for designing nano-scale computers: Exploring the state-of-the-art techniques and suggesting the opportunities for the future. *Optik* **2022**, *265*, 169431.
- (14) Beran, G. J. O. Frontiers of molecular crystal structure prediction for pharmaceuticals and functional organic materials. *Chemical Science* **2023**, *14*, 13290–13312.
- (15) Nassar, R.; Dignon, G. L.; Razban, R. M.; Dill, K. A. The Protein Folding Problem: The Role of Theory. *Journal of Molecular Biology* **2021**, *433*, 167126.
- (16) Li, Y.; Liang, D.; Wang, R.; Yang, S.; Liu, W.; Sang, Q.; Pu, J.; Wang, Y.; Qian, K. Interfacial Self-Assembly Nanostructures: Constructions and Applications. *Small* **2024**, *20*, 2405318.
- (17) Sumaiya, S. A.; Baykara, M. Z. Atomic-scale imaging and spectroscopy via scanning probe microscopy: An overview. *Journal of Vacuum Science & Technology B* **2023**, *41*, 060802.
- (18) Xiong, W.; Lu, J.; Geng, J.; Ruan, Z.; Zhang, H.; Zhang, Y.; Niu, G.; Fu, B.; Zhang, Y.; Sun, S.; Gao, L.; Cai, J. Atomic-scale construction and characterization of quantum dots array and polyfluorene chains via 2,7-dibromofluorene on Au(111). *Applied Surface Science* **2023**, *609*, 155315.
- (19) Scheidt, J.; Diener, A.; Maiworm, M.; Müller, K.-R.; Findeisen, R.; Driessens, K.; Tautz, F. S.; Wagner, C. Concept for the Real-Time Monitoring of Molecular Configurations during Manipulation with a Scanning Probe Microscope. *The Journal of Physical Chemistry C* **2023**, *127*, 13817–13836.
- (20) Leinen, P.; Esders, M.; Schütt, K. T.; Wagner, C.; Müller, K.-R.; Tautz, F. S. Autonomous robotic nanofabrication with reinforcement learning. *Science Advances* **2020**, *6*, eabb6987.
- (21) Ramsauer, B.; Simpson, G. J.; Cartus, J. J.; Jeindl, A.; García-López, V.; Tour, J. M.; Grill, L.; Hofmann, O. T. Autonomous Single-Molecule Manipulation Based on Reinforcement Learning. *The Journal of Physical Chemistry A* **2023**, *127*, 2041–2050.
- (22) Ramsauer, B.; Cartus, J. J.; Hofmann, O. T. MAM-STM: A software for autonomous control of single moieties towards specific surface positions. *Computer Physics Communications* **2024**, *303*, 109264.
- (23) Liang, J.; Makovychuk, V.; Handa, A.; Chentanez, N.; Macklin, M.; Fox, D.



- GPU-accelerated robotic simulation for distributed reinforcement learning. Conference on Robot Learning. 2018; pp 270–282.
- (24) Manikandan, M.; Nicolini, P.; Hapala, P. Computational Design of Photosensitive Polymer Templates To Drive Molecular Nanofabrication. *ACS Nano* **2024**, *18*, 9969–9979.
- (25) Jumper, J.; Evans, R.; Pritzel, A.; Green, T.; Figurnov, M.; Ronneberger, O.; Tunyasuvunakool, K.; Bates, R.; Židek, A.; Potapenko, A.; Bridgland, A.; Meyer, C.; Kohl, S. A. A.; Ballard, A. J.; Cowie, A.; Romera-Paredes, B.; Nikolov, S.; Jain, R.; Adler, J.; Back, T.; Petersen, S.; Reiman, D.; Clancy, E.; Zielinski, M.; Steinegger, M.; Pacholska, M.; Berghammer, T.; Bodenstein, S.; Silver, D.; Vinyals, O.; Senior, A. W.; Kavukcuoglu, K.; Kohli, P.; Hassabis, D. Highly accurate protein structure prediction with AlphaFold. *Nature* **2021**, *596*, 583–589.
- (26) wwPDB consortium Protein Data Bank: the single global archive for 3D macromolecular structure data. *Nucleic Acids Research* **2018**, *47*, D520–D528.
- (27) Pracht, P.; Grimme, S.; Bannwarth, C.; Bohle, F.; Ehlert, S.; Feldmann, G.; Gorges, J.; Müller, M.; Neudecker, T.; Plett, C.; Spicher, S.; Steinbach, P.; Wośowski, P. A.; Zeller, F. CREST—A program for the exploration of low-energy molecular chemical space. *The Journal of Chemical Physics* **2024**, *160*, 114110.
- (28) Wang, J.; Wolf, R. M.; Caldwell, J. W.; Kollman, P. A.; Case, D. A. Development and testing of a general amber force field. *Journal of Computational Chemistry* **2004**, *25*, 1157–1174.
- (29) Vanommeslaeghe, K.; Hatcher, E.; Acharya, C.; Kundu, S.; Zhong, S.; Shim, J.; Darian, E.; Guvench, O.; Lopes, P.; Vorobyov, I.; MacKerell Jr., A. D. CHARMM general force field: A force field for drug-like molecules compatible with the CHARMM all-atom additive biological force fields. *Journal of Computational Chemistry* **2010**, *31*, 671–690.
- (30) Oostenbrink, C.; Villa, A.; Mark, A. E.; Van Gunsteren, W. F. A biomolecular force field based on the free enthalpy of hydration and solvation: The GRO-MOS force-field parameter sets 53A5 and 53A6. *Journal of Computational Chemistry* **2004**, *25*, 1656–1676.
- (31) Jorgensen, W. L.; Maxwell, D. S.; Tirado-Rives, J. Development and Testing of the OPLS All-Atom Force Field on Conformational Energetics and Properties of Organic Liquids. *Journal of the American Chemical Society* **1996**, *118*, 11225–11236.
- (32) Case, D. A.; Cheatham III, T. E.; Darden, T.; Gohlke, H.; Luo, R.; Merz Jr., K. M.; Onufriev, A.; Simmerling, C.; Wang, B.; Woods, R. J. The Amber biomolecular simulation programs. *Journal of Computational Chemistry* **2005**, *26*, 1668–1688.
- (33) Hwang, W.; Austin, S. L.; Blondel, A.; Boittier, E. D.; Boresch, S.; Buck, M.; Buckner, J.; Caffisch, A.; Chang, H.-T.; Cheng, X.; Choi, Y. K.; Chu, J.-W.; Crowley, M. F.; Cui, Q.; Damjanovic, A.; Deng, Y.; Devereux, M.; Ding, X.; Feig, M. F.; Gao, J.; Glowacki, D. R.; Gonzales, J. E. I.; Hamaneh, M. B.; Harder, E. D.; Hayes, R. L.; Huang, J.; Huang, Y.; Hudson, P. S.; Im, W.; Islam, S. M.; Jiang, W.; Jones, M. R.; Käser, S.; Kearns, F. L.; Kern, N. R.; Klauda, J. B.; Lazaridis, T.; Lee, J.; Lemkul, J. A.; Liu, X.; Luo, Y.; MacKerell, A. D. J.; Major, D. T.; Meuwly, M.; Nam, K.; Nilsson, L.; Ovchinnikov, V.; Paci, E.; Park, S.; Pastor, R. W.; Pittman, A. R.; Post, C. B.;



- Prasad, S.; Pu, J.; Qi, Y.; Rathinavelan, T.; Roe, D. R.; Roux, B.; Rowley, C. N.; Shen, J.; Simmonett, A. C.; Sodt, A. J.; Töpfer, K.; Upadhyay, M.; van der Vaart, A.; Vazquez-Salazar, L. I.; Venable, R. M.; Warrensford, L. C.; Woodcock, H. L.; Wu, Y.; Brooks, C. L. I.; Brooks, B. R.; Karplus, M. CHARMM at 45: Enhancements in Accessibility, Functionality, and Speed. *The Journal of Physical Chemistry B* **2024**, *128*, 9976–10042.
- (34) Abraham, M. J.; Murtola, T.; Schulz, R.; Páll, S.; Smith, J. C.; Hess, B.; Lindahl, E. GROMACS: High performance molecular simulations through multi-level parallelism from laptops to supercomputers. *SoftwareX* **2015**, *1–2*, 19–25.
- (35) Thompson, A. P.; Aktulga, H. M.; Berger, R.; Bolintineanu, D. S.; Brown, W. M.; Crozier, P. S.; in 't Veld, P. J.; Kohlmeyer, A.; Moore, S. G.; Nguyen, T. D.; Shan, R.; Stevens, M. J.; Tranchida, J.; Trott, C.; Plimpton, S. J. LAMMPS - a flexible simulation tool for particle-based materials modeling at the atomic, meso, and continuum scales. *Computer Physics Communication* **2022**, *271*, 108171.
- (36) Phillips, J. C.; Hardy, D. J.; Maia, J. D. C.; Stone, J. E.; Ribeiro, J. V.; Bernardi, R. C.; Buch, R.; Fiorin, G.; Hénin, J.; Jiang, W.; McGreevy, R.; Melo, M. C. R.; Radak, B. K.; Skeel, R. D.; Singharoy, A.; Wang, Y.; Roux, B.; Aksimentiev, A.; Luthey-Schulten, Z.; Kalé, L. V.; Schulten, K.; Chipot, C.; Tajkhorshid, E. Scalable molecular dynamics on CPU and GPU architectures with NAMD. *The Journal of Chemical Physics* **2020**, *153*, 044130.
- (37) FireCore. <https://github.com/ProkopHapala/FireCore>, Accessed: 23/07/2025.
- (38) In LAMMPS this can be easily done using the `neigh_modify exclude` command, while in the other codes there is generally no native support, even though workarounds exist.
- (39) Ewald, P. P. Die Berechnung optischer und elektrostatischer Gitterpotentiale. *Annalen der Physik* **1921**, *369*, 253–287.
- (40) Darden, T.; York, D.; Pedersen, L. Particle mesh Ewald: An N-log(N) method for Ewald sums in large systems. *The Journal of Chemical Physics* **1993**, *98*, 10089–10092.
- (41) Pattabiraman, N.; Levitt, M.; Ferrin, T. E.; Langridge, R. Computer graphics in real-time docking with energy calculation and minimization. *Journal of Computational Chemistry* **1985**, *6*, 432–436.
- (42) Meng, E. C.; Shoichet, B. K.; Kuntz, I. D. Automated docking with grid-based energy evaluation. *Journal of Computational Chemistry* **1992**, *13*, 505–524.
- (43) Grimme, S.; Antony, J.; Ehrlich, S.; Krieg, H. A consistent and accurate ab initio parametrization of density functional dispersion correction (DFT-D) for the 94 elements H-Pu. *The Journal of Chemical Physics* **2010**, *132*, 154104.
- (44) Ellner, M.; Pou, P.; Pérez, R. Molecular Identification, Bond Order Discrimination, and Apparent Intermolecular Features in Atomic Force Microscopy Studied with a Charge Density Based Method. *ACS Nano* **2019**, *13*, 786–795.
- (45) Oinonen, N.; Yakutovich, A. V.; Gallardo, A.; Ondráček, M.; Hapala, P.; Krejčí, O. Advancing scanning probe microscopy simulations: A decade of development in probe-particle models. *Computer Physics Communications* **2024**, *305*, 109341.
- (46) Friesner, R. A.; Banks, J. L.; Murphy, R. B.; Halgren, T. A.; Klicic, J. J.; Mainz, D. T.; Repasky, M. P.; Knoll, E. H.; Shelley, M.; Perry, J. K.; Shaw, D. E.; Francis, P.; Shenkin, P. S.

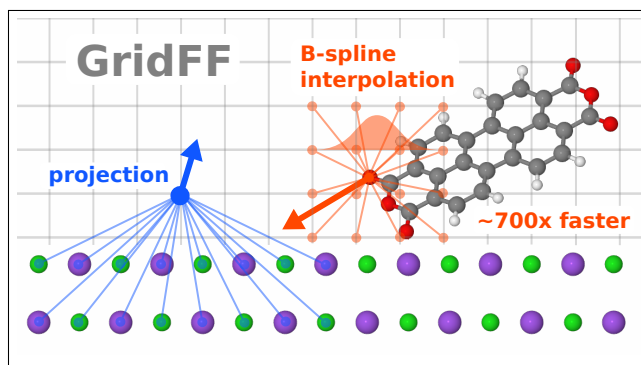
- Glide: A New Approach for Rapid, Accurate Docking and Scoring. 1. Method and Assessment of Docking Accuracy. *Journal of Medicinal Chemistry* **2004**, *47*, 1739–1749.
- (47) Allen, W. J.; Balias, T. E.; Mukherjee, S.; Brozell, S. R.; Moustakas, D. T.; Lang, P. T.; Case, D. A.; Kuntz, I. D.; Rizzo, R. C. DOCK 6: Impact of new features and current docking performance. *Journal of Computational Chemistry* **2015**, *36*, 1132–1156.
- (48) Eberhardt, J.; Santos-Martins, D.; Tillack, A. F.; Forli, S. AutoDock Vina 1.2.0: New Docking Methods, Expanded Force Field, and Python Bindings. *Journal of Chemical Information and Modeling* **2021**, *61*, 3891–3898.
- (49) Goodford, P. J. A computational procedure for determining energetically favorable binding sites on biologically important macromolecules. *Journal of Medicinal Chemistry* **1985**, *28*, 849–857.
- (50) Diller, D. J.; Verlinde, C. L. M. J. A critical evaluation of several global optimization algorithms for the purpose of molecular docking. *Journal of Computational Chemistry* **1999**, *20*, 1740–1751.
- (51) Oberlin, D.; Scheraga, H. A. B-spline method for energy minimization in grid-based molecular mechanics calculations. *Journal of Computational Chemistry* **1998**, *19*, 71–85.
- (52) Minh, D. D. L. Power transformations improve interpolation of grids for molecular mechanics interaction energies. *Journal of Computational Chemistry* **2018**, *39*, 1200–1207.
- (53) Tomioka, N.; Itai, A. GREEN: A program package for docking studies in rational drug design. *Journal of Computer-Aided Molecular Design* **1994**, *8*, 347–366.
- (54) Venkatachalam, C. M.; Jiang, X.; Oldfield, T.; Waldman, M. LigandFit: a novel method for the shape-directed rapid docking of ligands to protein active sites. *Journal of Molecular Graphics and Modelling* **2003**, *21*, 289–307.
- (55) Forouzesh, N.; Izadi, S.; Onufriev, A. V. Grid-Based Surface Generalized Born Model for Calculation of Electrostatic Binding Free Energies. *Journal of Chemical Information and Modeling* **2017**, *57*, 2505–2513.
- (56) Minh, D. D. L. Alchemical Grid Dock (AlGDock): Binding Free Energy Calculations between Flexible Ligands and Rigid Receptors. *Journal of Computational Chemistry* **2020**, *41*, 715–730.
- (57) Ren, E.; Coudert, F.-X. Enhancing Gas Separation Selectivity Prediction through Geometrical and Chemical Descriptors. *Chemistry of Materials* **2023**, *35*, 6771–6781.
- (58) Wu, G.; Robertson, D. H.; Brooks III, C. L.; Vieth, M. Detailed analysis of grid-based molecular docking: A case study of CDOCKER—A CHARMM-based MD docking algorithm. *Journal of Computational Chemistry* **2003**, *24*, 1549–1562.
- (59) Yeh, I.-C.; Berkowitz, M. L. Ewald summation for systems with slab geometry. *The Journal of Chemical Physics* **1999**, *111*, 3155–3162.
- (60) Arnold, A.; Fahrenberger, F.; Holm, C.; Lenz, O.; Bolten, M.; Dachsel, H.; Halver, R.; Kabadshow, I.; Gähler, F.; Heber, F.; Iseringhausen, J.; Hofmann, M.; Pippig, M.; Potts, D.; Sutmman, G. Comparison of scalable fast methods for long-range interactions. *Physical Review E* **2013**, *88*, 063308.
- (61) Soler, J. M.; Artacho, E.; Gale, J. D.; García, A.; Junquera, J.; Ordejón, P.; Sánchez-Portal, D. The SIESTA method for ab initio order-N materials simulation. *Journal of Physics: Condensed Matter* **2002**, *14*, 2745.

- (62) Kresse, G.; Furthmüller, J. Efficient iterative schemes for ab initio total-energy calculations using a plane-wave basis set. *Physical Review B* **1996**, *54*, 11169–11186.
- (63) Hapala, P.; Temirov, R.; Tautz, F. S.; Jelínek, P. Origin of High-Resolution IETS-STM Images of Organic Molecules with Functionalized Tips. *Physical Review Letters* **2014**, *113*, 226101.
- (64) Trosset, J.-Y.; Scheraga, H. A. Reaching the global minimum in docking simulations: A Monte Carlo energy minimization approach using Bezier splines. *Proceedings of the National Academy of Sciences* **1998**, *95*, 8011–8015.
- (65) Karacuban, H.; Koch, S.; Fendrich, M.; Wagner, T.; Möller, R. PTCDA on Cu(111) partially covered with NaCl. *Nanotechnology* **2011**, *22*, 295305.
- (66) Swart, I.; Sonnleitner, T.; Niedenführ, J.; Repp, J. Controlled Lateral Manipulation of Molecules on Insulating Films by STM. *Nano Letters* **2012**, *12*, 1070–1074.
- (67) de Campos Ferreira, R. C.; Sagwal, A.; Doležal, J.; Canola, S.; Merino, P.; Neuman, T.; Švec, M. Resonant Tip-Enhanced Raman Spectroscopy of a Single-Molecule Kondo System. *ACS Nano* **2024**, *18*, 13164–13170.
- (68) Bayly, C. I.; Cieplak, P.; Cornell, W.; Kollman, P. A. A well-behaved electrostatic potential based method using charge restraints for deriving atomic charges: the RESP model. *The Journal of Physical Chemistry* **1993**, *97*, 10269–10280.
- (69) Bader, R. F. W. *Atoms in Molecules: a Quantum Theory*; Oxford University Press: New York, 1990.
- (70) Rappe, A. K.; Casewit, C. J.; Colwell, K. S.; Goddard, W. A. I.; Skiff, W. M. UFF, a full periodic table force field for molecular mechanics and molecular dynamics simulations. *Journal of the American Chemical Society* **1992**, *114*, 10024–10035.
- (71) Hockney, R.; Eastwood, J. *Computer Simulation Using Particles*; Adam Hilger: New York, 1988.
- (72) Bitzek, E.; Koskinen, P.; Gähler, F.; Moseler, M.; Gumbusch, P. Structural Relaxation Made Simple. *Physical Review Letters* **2006**, *97*, 170201.
- (73) Ouyang, W.; Mandelli, D.; Urbakh, M.; Hod, O. Nanoserpents: Graphene Nanoribbon Motion on Two-Dimensional Hexagonal Materials. *Nano Letters* **2018**, *18*, 6009–6016.
- (74) Vilhena, J. G.; Pawlak, R.; D’Astolfo, P.; Liu, X.; Gnecco, E.; Kisiel, M.; Glatzel, T.; Pérez, R.; Häner, R.; Decurtins, S.; Baratoff, A.; Prampolini, G.; Liu, S.-X.; Meyer, E. Flexible Superlubricity Unveiled in Sidewinding Motion of Individual Polymeric Chains. *Physical Review Letters* **2022**, *128*, 216102.
- (75) GridFF folder. [https://github.com/ProkopHapala/FireCore/tree/debug/grid\\_generation\\_and\\_test/tests/tGridFF](https://github.com/ProkopHapala/FireCore/tree/debug/grid_generation_and_test/tests/tGridFF), Accessed: 23/07/2025.
- (76) Rappe, A. K.; Goddard, W. A. Charge equilibration for molecular dynamics simulations. *The Journal of Physical Chemistry* **1991**, *95*, 3358–3363.
- (77) Lewis, J. P.; Jelínek, P.; Ortega, J.; Demkov, A. A.; Trabada, D. G.; Haycock, B.; Wang, H.; Adams, G.; Tomfohr, J. K.; Abad, E.; Wang, H.; Drabold, D. A. Advances and applications in the Fjscpl/IREBALL/scplab initio tight-binding molecular-dynamics formalism. *physica status solidi (b)* **2011**, *248*, 1989–2007.
- (78) Mendieta-Moreno, J. I.; Walker, R. C.; Lewis, J. P.; Gómez-Puertas, P.; Mendieta, J.; Ortega, J. FIREBALL/AMBER: An Efficient Local-Orbital DFT QM/MM

Method for Biomolecular Systems. *Journal of Chemical Theory and Computation* **2014**, *10*, 2185–2193.

- (79) Evans, W. A. B.; Heyes, D. M.; Powles, J. G.; Rickayzen, G. Parametrization of linear dielectric response. *Physical Review E* **2011**, *83*, 046601.
- (80) Tabacchi, G.; Mundy, C. J.; Hutter, J.; Parrinello, M. Classical polarizable force fields parametrized from ab initio calculations. *The Journal of Chemical Physics* **2002**, *117*, 1416–1433.
- (81) Harshan, A. K.; Bronson, M. J. J.; Jensen, L. Local-Field Effects in Linear Response Properties within a Polarizable Frozen Density Embedding Method. *Journal of Chemical Theory and Computation* **2022**, *18*, 380–393.
- (82) Piegl, L.; Tiller, W. *The NURBS book*; Springer: Berlin, 1997.

# TOC Graphic



For Table of Contents Only